Vat 3D Printing of Bio-Derivable Photoresins – Towards Sustainable and Robust Thermoplastic Parts

Kyle C. H. Chin,[1†] Jianxun Cui,[2†] Robert M. O'Dea,[3†] Thomas H. Epps, III,[3,4,5*] Andrew J. Boydston[1,2,6*]

[1]*Department of Chemical and Biological Engineering, University of Wisconsin, Madison, WI, 53706, USA*

[2]*Department of Chemistry, University of Wisconsin, Madison, WI, 53706, USA*

[3]*Department of Chemical and Biomolecular Engineering, University of Delaware, Newark, Delaware 19716, USA*

[4]*Department of Materials Science and Engineering, University of Delaware, Newark, Delaware 19716, USA*

[5]*Center for Research in Soft matter and Polymers (CRiSP), University of Delaware, Newark, Delaware 19716, USA*

[6]*Department of Materials Science and Engineering, University of Wisconsin, Madison, WI, 53706, USA*

[†]*These authors contributed equally to this work; listed alphabetically by last name*

**Co-corresponding authors, email: thepps@udel.edu, aboydston@wisc.edu*

Abstract

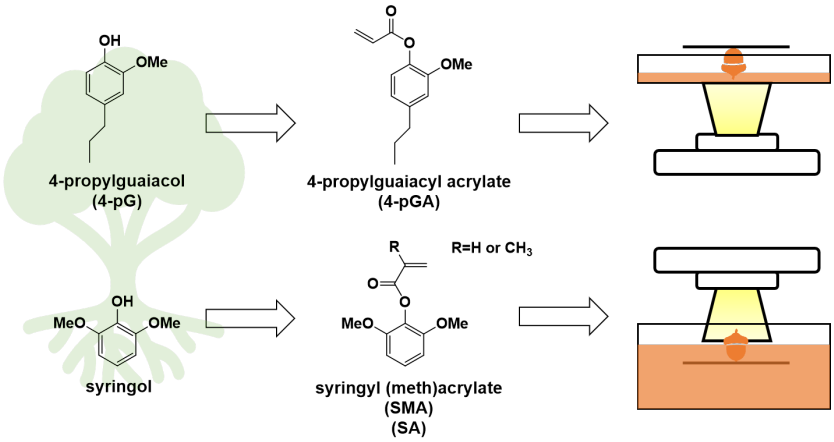

Vat photopolymerization 3D printing (3DP) of thermoplastic materials is exceedingly difficult due to the typical reliance on crosslinking on a timescale relevant to form well-defined, solid objects. Additionally, photoresin build materials overwhelmingly rely upon non-renewable feedstocks. To address these challenges, we report the vat 3DP of bio-derivable photoresins that produced thermoplastic parts with highly tunable thermal and mechanical properties. The photoresins were formulated from two monomers that are easily obtainable from lignin deconstruction: 4-propylguaiacyl acrylate (4-pGA) and syringyl methacrylate (SMA). These bio-derivable materials

generated printed parts that ranged from soft elastomers to rigid plastics. For example, for 4-pGA-based materials, the breaking stresses varied from 0.20 to 20 MPa and breaking strains could be tuned from 4.7% up to 1700%, whereas SMA-based materials resulted in higher breaking stresses (~30 MPa) and T_gs (~132 °C). Notably, parts printed from these bio-derivable formulations exhibited thermoplastic behavior and were largely soluble in common organic solvents—expanding the application and repurposing of the 3D-printed parts. We highlight this feature by reusing a 3DP part *via* solvent casting. Overall, the tunable properties and thermoplastic behavior of the lignin-derivable photoresins showcase renewable lignin resources as promising biofeedstocks for sustainable 3DP.

Introduction

Using 3D printing (3DP) technologies, objects can be efficiently constructed from digital models, affording increased flexibility in design and functionality. 3DP has found broad application in medical devices,[1,2] transportation,[3] electronics,[4] robotics,[5–7] and other fields.[8,9] Among the different 3DP techniques, vat photopolymerization builds solid 3D objects through patterned layer-by-layer curing of a liquid photoresin.[10] These patterns are created from light delivered *via* either 2D projections or rastering lasers.[10] Objects also can be constructed volumetrically by projecting a directed light dosage into the resin.[11,12] The advantages of vat photopolymerization include high feature resolution, comparatively fast print times, and direct access to overhangs and hollow voids without supports.[10]

Vat photopolymerization resins typically consists of a monofunctional monomer, a multifunctional monomer, and a photoinitiation system.[10,13–15] Although these are the base components, more complex resins can include fillers, additives, and dyes that enhance the properties or resolution of the printed parts.[10] Because the macromolecular scaffold is created from precursor monomer during the photocuring process, the resin components must have high polymerization rates, and often, crosslinking is required to reach rapid gelation at low conversions. Hence, the vast majority of photoresin monomers comprise acrylate and methacrylate functionalities because their rapid cure times reduce the amount of crosslinker needed to produce quality parts. Additionally, the need for low viscosity resins precludes the use of viscous components, such as oligomers, that could aid in forming fixity and improve the final properties of printed parts.[10] The above constraints typically result in networks that exhibit inferior mechanical and thermal properties in comparison to commodity and high-performance plastics polymerized *via* conventional techniques (*e.g.,* bulk or solution free-radical, controlled-radical, or ionic polymerization).[10,16] Thus, photoresin systems that can produce parts using 3DP techniques without compromising the thermal and mechanical properties of the materials are highly desirable.

Sustainability also is a key metric for printable resin formulations; however, most commercial monomers for vat photopolymerization 3DP are obtained from finite and non-renewable, petroleum-based chemicals. Renewable alternatives could enhance materials sustainability.[17] One promising strategy for more environmentally friendly monomer sourcing is the deconstruction of lignocellulosic biomass, especially lignin.[18–22] Lignin is the second most abundant biopolymer behind cellulose and is reported to account for about 30% of the organic carbon in the biosphere,[23] making it an ideal candidate to replace petrochemical sources.

The molecular structure of lignin results in a highly crosslinked and amorphous aromatic network; however, despite its recalcitrant nature, lignin can be deconstructed to produce a variety of small

molecule aromatic compounds that are useful as building blocks for new value-added chemicals, pharmaceuticals, fuels, and polymers.[18,24–26] Macromolecular products based on lignin-derived starting materials have already demonstrated performance-advantaged characteristics in various areas, such as the production of elastomers,[26,27] commodity plastics,[17] epoxy resins,[25,28,29] high-T_g (glass transition temperature) materials,[30,31] and pressure-sensitive adhesives (PSAs).[32]

Herein, we investigated the 3DP of lignin-derivable photoresin formulations using vat photopolymerization. Our monomer pool was selected from recent reports that highlighted acrylate-based monomers produced from feedstocks accessible through lignin deconstruction.[31,32] For example, the above-mentioned, high-performance PSAs were generated using 4-propylguiaicyl acrylate (4-pGA) as a key component, illustrating their potential use as robust elastomers.[32] As another example, attractive features of polymers synthesized from bio-derivable syringyl methacrylate (SMA) include high T_gs (205 °C) that exceed those typically achievable with vat photopolymerization 3DP.[31]

Results and discussion

3D printing of 4-pGA- and SMA-based resins

Motivated by previous work on lignin-derived (meth)acrylates, we selected 4-propylguaiacol (4-pG) and syringol as starting materials for our development of biobased 3DP resins.[31,32] We employed standard synthetic manipulations to convert 4-pG to 4-pGA and syringol to SMA (Figure 1).[32] Our studies also made use of syringyl acrylate (SA), lauryl acrylate (LA), lauryl methacrylate (LMA), and Irgacure 819 (Irg 819) as depicted in Figure 1.

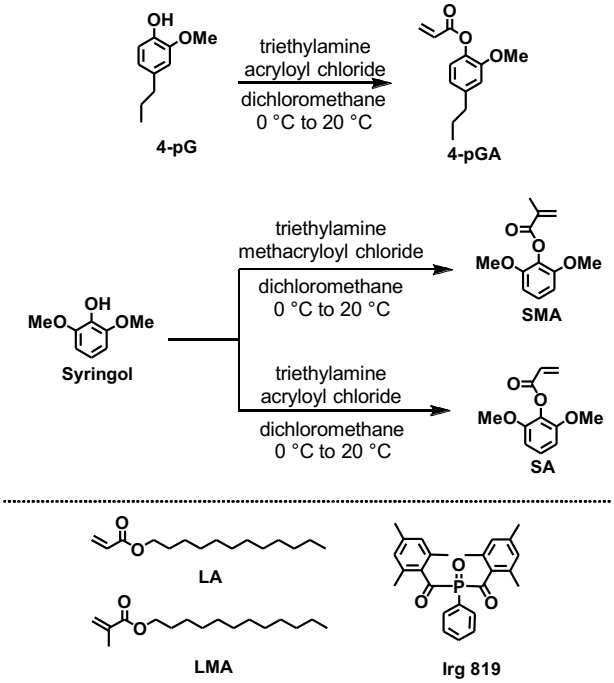

Figure 1. Top) Route for conversion of 4-pG and syringol into 4-pGA, SMA, and SA monomers for 3DP. Bottom) Illustration of LA, LMA, and Irg 819 molecules, which are additional species used in this investigation.

To gauge the general characteristics of the 4-pGA and SMA resins, we performed bulk curing screens of each monomer using Irg 819 as the photoinitiator. Each resin system yielded optically transparent materials (Figure 2, top). We found that homopolymerization of 4-pGA resulted in qualitatively stiff, brittle specimens. Thus, LA was incorporated as a comonomer to reduce brittleness, resulting in slightly tacky samples that could be stretched to high strains without breaking (Figure 2, middle). Post stretch, the samples took ~1 h to relax back to their original shape. In addition to imparting high flexibility to the printed parts, LA offers low volatility, and it can be produced from sustainable sources.[33,34] Homopolymerization of SMA also resulted in stiff, brittle specimens but had the benefit of producing high T_g samples (Figure 2, bottom).[31]

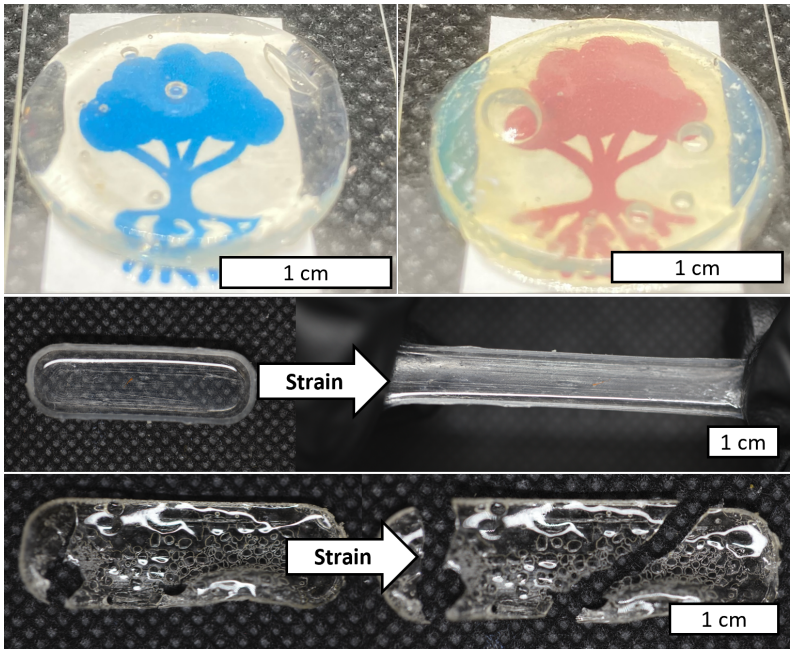

Figure 2. Top) Cured drops of 4-pGA-3(left) and SMA-1 (right) resin. Middle) 4-pGA-3 resin cured into a rectangle and stretched to large strains. Bottom) SMA-1 resin cured into a rectangle. Sample broke upon stretching showing its stiff and brittle nature.

Following the bulk curing experiments, we transitioned to vat photopolymerization 3DP. Photoresins with 4-pGA as the primary component were printed using a bottom-up printing setup (Figure S1). We found that the addition of 4-pG as an inhibitor was effective at suppressing overgrowth during printing, which offered a practical solution given that 4-pG was already part of the sustainable resin sourcing. Although SMA is a solid at room temperature, it has a melting point of 40 °C. Thus, we implemented a top-down printer configuration (images were projected from above the vat) that enabled heating of the resin vat in a water bath that was set to 40 °C (Figure S2). For prints using SMA as the main component, we again employed 4-pG as an inhibitor. Layer cure times for each resin were systematically determined by illuminating photoresins with sequentially longer light exposures until solid material remained after washing away any uncured material with isopropyl alcohol (Figure S3, Table S1). Using this approach, parts could be printed with good resolution (*i.e.,* small feature sizes) and complex geometries, such as voids and overhangs (Figure 3, Figure S4). While resolution varied depending on resin, in general, dimensional accuracy of 400 µm was achieved and features sizes as small as 500 µm were achieved (Figure S5).

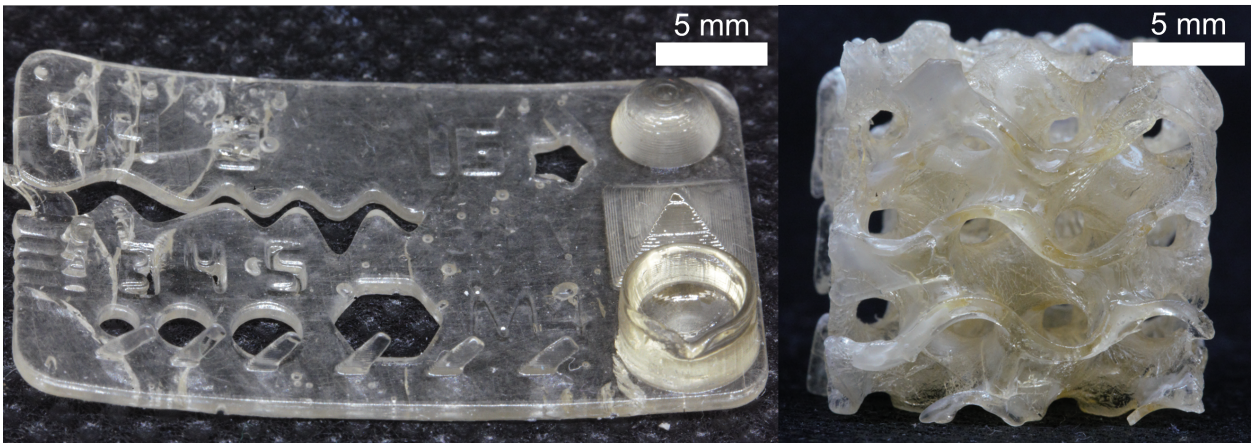

Figure 3. Printed objects from SMA-3 resin. The left object illustrates the ability to achieve good resolution with small features. The right object is a complex lattice architecture that would be difficult to produce with non-additive techniques.

Thermal and mechanical properties of parts produced from 4-pGA-based resins

Table 1. Summarized compositions and thermal and mechanical properties for 4-pGA resins. The data shown for mechanical testing are the mean and standard deviation for five replicate experiments. Note: Of the five samples tested for 4-pGA-4, two broke, whereas the other three hit the maximum strain of the instrument (~2000%). In this case, the maximum strain and corresponding stress were used for calculations.

Resin	4-pGA (wt %)[a]	LA (wt %)[a]	SA (wt %)[a]	Breaking strain (%)	Breaking stress (MPa)	Yield stress (MPa)	T_g (°C)	$T_{g,theo}$ (°C)
4-pGA-1	91	9	0	220 ± 30	7.1 ± 0.6	10.1 ± 0.5	18	27
4-pGA-2	83	17	0	298 ± 9	4.4 ± 0.5	2.70	12	17
4-pGA-3	66	34	0	680 ± 30	1.53 ± 0.06	--	1	-1
4-pGA-4	50	50	0	1700 ± 100	0.20 ± 0.06	--	-15	-17
4-pGA-5	25	50	25	600 ± 30	1.4 ± 0.2	--	1	-6
4-pGA-6	60	10	30	4.7 ± 0.9	20± 2	--	38	43

[a]Weight percent of monomer component [*]All resins contained 0.04 wt % 4-pG as inhibitor and 0.2 wt % Irg 819 as photoinitiator relative to the total monomer weight. Theoretical T_gs ($T_{g,theo}$) were determined from the Fox equation with experimentally determined T_gs for 4-pGA and SA and the literature value T_g for LA.

With printability confirmed, we focused on understanding the mechanical properties of the printed parts. We determined that the tensile mechanical properties can be tuned dramatically by changing the feed ratio of 4-pGA and LA (Figure 4A, Table 1). For example, 4-pGA-1 printed samples were rigid, yielded under tension, showed large plastic deformation (220%), and displayed strain hardening beyond the yield point. As the fraction of LA was systematically increased (cf. 4-pGA-1 through 4-pGA-4), the printed specimens became more ductile, likely due to the long aliphatic sidechain of LA increasing chain mobility and free volume. The yield stress decreased across this series with concomitant increases in breaking strain. At higher loadings of LA (4-pGA-3 and 4-

pGA-4), the stress-strain curves exhibited characteristics of a soft elastomer, with breaking strains reaching as high as 677% and 1700%, respectively. We also briefly investigated the influence of SA in the photoresin formulation. Adding SA offered an opportunity for fine-tuning of mechanical properties (Figure 4A, Table 2). In the case of soft elastomers (4-pGA-4), partial displacement of 4-pGA with SA (4-pGA-5) resulted in stiffer products with lower breaking strain. In the case of rigid materials (4-pGA-1), the addition of SA increased the breaking stress, albeit at the expense of ductility (4-pGA-6).

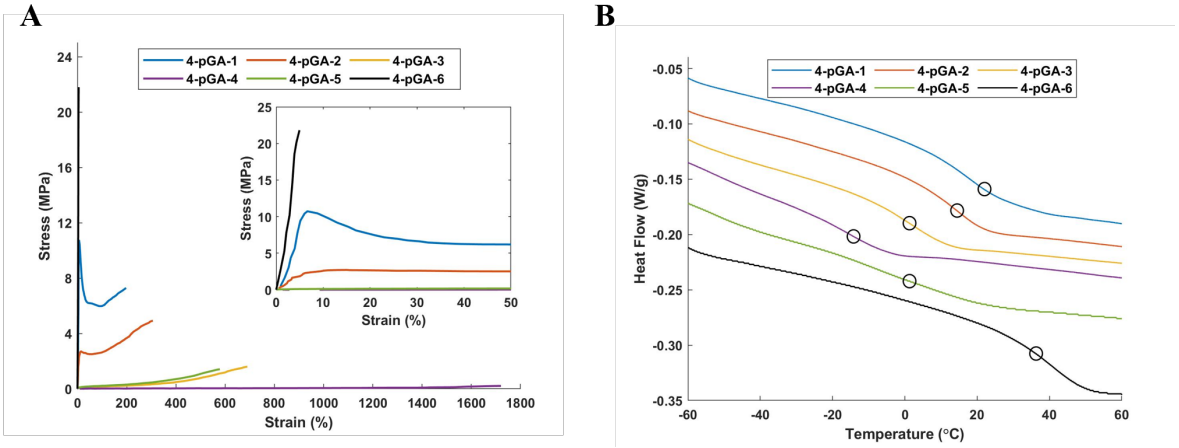

Figure 4. A) Representative stress-strain curves of parts produced from 4-pGA-based resin formulations. Inset plot shows a zoomed-in section from 0 to 50 % strain. B) Representative differential scanning calorimetry (DSC) traces of the second heating cycle to illustrate the shift in T_g of parts produced from 4-pGA-based resins. T_g of each sample is circled. Curves are shifted vertically for clarity in panel B.

The thermal properties of the printed 4-pGA-based parts were assessed by differential scanning calorimetry (DSC) (Figure 4B, Table 2). Monomers 4-pGA and SA were each homopolymerized *via* uncontrolled radical polymerization; the resulting polymers exhibited T_gs of 38 and 113 °C, respectively (Figure S6). Homopolymerization of LA produced a free-flowing polymer melt, indicating it would not be suitable for 3DP as a homopolymer. Poly(lauryl acrylate) has a reported T_g of -55 °C. [35] In general, the T_g of printed parts decreased with increasing amounts of LA with a range of -15 to 38 °C. In each case, we noted a single T_g, consistent with a homogenous, statistical distribution of comonomers (as opposed to block-like microstructures). Additionally, the inclusion of SA at the expense of 4-pGA in the formulation increased the T_g (*e.g.,* 4-pGA-1 versus 4-pGA-6, 4-pGA-4 versus 4-pGA-5). These trends align with theoretical predictions of T_g for each resin compositions determined using the Fox equation (Table 1).[36] 4-pGA-1 and 4-pGA-6 were also characterized by dynamic mechanical analysis (DMA) to assess their thermomechanical properties (Figure S7**)**. No obvious rubbery plateaus were present in the temperature range measured (23 – 100 °C). For 4-pGA-1, the storage modulus began decreasing around the T_g, 18 °C, with a more extreme drop at approximately 40 °C. Replacing some 4-pGA with SA (4-pGA-6) shifted the corresponding transitions to 38 and 50 °C, respectively. The values measured by DMA were consistent with the T_g trends determined by DSC.

Thermal and mechanical properties of parts produced from SMA-based resins

We also printed a series of specimens for uniaxial tensile testing of SMA-based samples. We chose to focus on SMA over SA given that homopolymers of SMA led to parts with higher T_gs, and therefore SMA provides an upper bound on thermal properties in our studies. The parts produced from SMA-1 with a post-cure at 40 °C for 1 h were very brittle (breaking strain of only 2%) and weak (breaking stress of only 7 MPa) (Figure S8, Table 2), and they did not show any plastic deformation before break. Attempts to toughen the materials by adding LMA to the formulation (SMA-2) were unsuccessful, as the breaking strain and stress were still low (breaking strain of only 3% and breaking stress of only 2 MPa) (Figure S8, Table 2).

Table 2. Summary of mechanical properties under tension (SMA-1 post-cure 40 °C and SMA-2) and compression (SMA-1 post-cure 140 °C and SMA-3) along with thermal data determined by DSC. The data shown for mechanical testing are the mean and standard deviation for five replicate experiments.

Resin[a]	SMA (wt %)[b]	LMA (wt %)[b]	Irg 819 (wt %)[c]	Post-cure temperature (°C)	Breaking strain (%)	Breaking stress (MPa)	T_g (°C)
SMA-1^T	100	0	0.2	40	1.7 ± 0.4	7 ± 1	166[d]
SMA-1^C	100	0	0.2	140	2.4 ±0.4	30 ± 9	122
SMA-2^T	50	50	0.2	40	3 ± 1	1.9 ± 0.6	--[e]
SMA-3^C	100	0	1	140	1.9 ± 0.3	30 ± 8	132

[a]Superscript T = analysis done under uniaxial tension; superscript C = analysis done under uniaxial compression. [b]Weight percent of monomer component. [c]Weight percent with respect to total monomer components. [d]DSC measurement obtained from a precipitated sample. [e]No definable T_g from DSC traces likely due to undercuring.

For samples printed using SMA-1 postcured at 40 °C, multiple glass transitions were detected by DSC, which is indicative of under-curing and plasticization, presumably by remaining monomer and oligomers (Figure S9). After dissolving these SMA-1 printed parts in dichloromethane and precipitating the polymer by adding the solution to excess methanol, the T_g increased to 166 °C (Figure S9). To improve the degree of curing, SMA-1 samples were post-cured at 140 °C, instead of 40 °C. After this adjustment, the printed part only exhibited a single T_g of 122 °C (Figure S9). Extending the 140 °C post-curing time beyond 1 h resulted in only small increases in T_g (Figure S10). Further adjustment of the formulation (SMA-3) by adding additional photoinitiator gave parts with a T_g of 132 °C (Figure S11). After post-curing at 140 °C, SMA specimens became more brittle, likely due to reduced plasticization, making the thin tensile testing samples unsuitable for analysis. Thus, printed cylinders were assessed under uniaxial compression. SMA-1 with 140 °C post-cure and SMA-3 gave similar results, with compressive breaking strains of 2% and compressive strengths of 30 MPa (Figure S12, Table 2).

DMA was used to evaluate the thermomechanical performance of SMA-1 and SMA-3 printed parts. The SMA specimens exhibited stable storage moduli at high temperature consistent with their high T_g values (Figure 5). A drop in storage modulus occurred above 100 °C for SMA-1 postcured at 140 °C. Increasing the percentage of photoinitiator (SMA-3) further increased the storage modulus and pushed the drop in storage modulus up to 140 °C. The impact of post-cure is evident in the DMA results for these two resins with the SMA-1 sample postcured at 140 °C retaining its storage modulus up to much higher temperatures than samples postcured at 40 °C

(Figure 5). The DMA results demonstrate that parts printed with SMA can retain their mechanical properties at temperatures significantly above 100 °C.

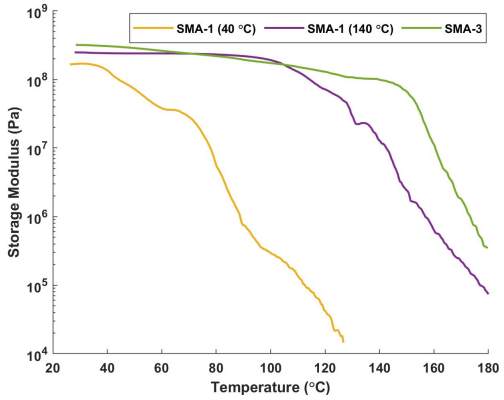

Figure 5. DMA data showing the storage modulus versus temperature for relevant printed SMA-based resins.

Reprocessability of 4-pGA and SMA thermoplastics

Although each of the aforementioned resin systems were printed without the use of crosslinkers, we still found good fixity of solid layers during printing. Most commonly, vat photopolymerization 3DP overwhelmingly produces thermoset parts due to the deliberate incorporation of crosslinkers, which give part fixity at low monomer conversion. Notably, vat photopolymerization 3DP of thermoplastics is rare because it requires striking a difficult balance between polymerization and polymer solubility.[37] The gelation during polymerization of monofunctional acrylates has been reported in bulk polymerization, but it is usually attributed to a reaction that is specific to the side chain of the acrylate or an alternative crosslinking mechanism such as branching and chain combination.[38,39] In our case, the creation of a thermoset was not necessary, and when the samples made with SMA-3 or 4-pGA-3 were placed in dichloromethane, they appeared to fully dissolve within 1 and 24 h, respectively (Figure S13).

To further investigate the nature of the thermoplastics, samples were printed from each resin, and molecular weight distributions were measured using size exclusion chromatography (SEC) with a chloroform mobile phase, a refractive index detector, and calibration against polystyrene standards. All of the printed samples exhibited relatively high molecular weights and broad dispersities—consistent with uncontrolled photoinitiated radical polymerizations (Table 3, Figure S14).[40] The two families of resin formulations led to considerably different solubilities of their respective printed parts, in agreement with previous literature reports (Table S2).[41] For instance, SMA-3 gave products that were soluble in dichloromethane and chloroform but insoluble in the other solvents that we tested. In contrast, products from 4-pGA-3 were found to be soluble in a range of organic solvents, including chlorinated solvents, ethers, hydrocarbons, and terpenes. The solubility in food-grade terpenes presents an opportunity for hazard reduction associated with parts clean-up and post-print treatments.

Table 3. SEC results from printed samples dissolved in chloroform using polystyrene standards.

Formulation	M_n (kDa)	M_w (kDa)	$Đ$
4-pGA-1	487	1,390	2.9
4-pGA-2	421	1,320	3.1
4-pGA-3	257	1,010	3.9
4-pGA-4	304	877	2.9
4-pGA-5	350	1,030	2.9
4-pGA-6[a]	111	626	5.6
SMA-1	193	449	2.3
SMA-2	85.3	312	3.7
SMA-3	58.8	303	5.2

[a] *Solubility was obtained by using higher purity LA*

The ability to print thermoplastic polymers in vat photopolymerization is rare and offers multiple advantages in sustainability and application. For example, the recycling options for printed thermoset objects are limited. However, parts prepared from 4-pGA- and SMA-based resins can be dissolved and repurposed using simple reprocessing steps such as solvent casting. To illustrate the potential recyclability of biobased prints, the parts were dissolved in dichloromethane and solvent casted into leaf molds (Figure 6). More broadly, one can envision using vat photopolymerization 3DP of thermoplastics to create sacrificial molds or for investment casting. Both of these important manufacturing methods can be made more accessible with 3DP, streamlining the fabrication of parts.[37,42–44]

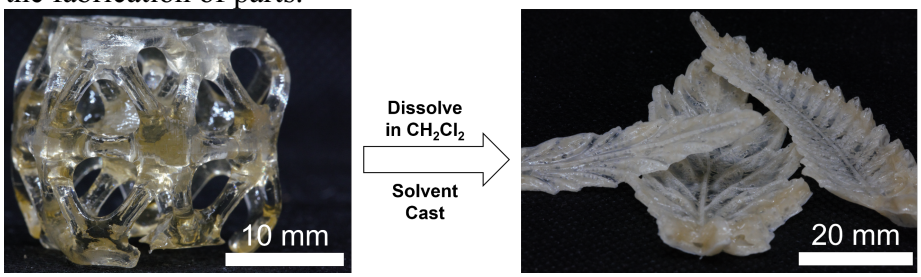

Figure 6. Illustration of the ability to solvent cast printed parts. A 3D-printed lattice from SMA-3 was dissolved in dichloromethane. The dissolved polymer could then be poured into a leaf mold, and the solvent evaporated away.

Conclusions

The 3D printing of a series of photoresin formulations using lignin-derivable monomers was reported. The thermomechanical properties of the resulting materials were characterized, and straightforward adjustments to monomer composition were leveraged to generate materials ranging from rigid plastics to soft and stretchable elastomers. Notably, each series of resins was printed without the use of crosslinker and resulted in thermoplastic parts. The thermoplastic properties enabled reprocessing of printed parts by solvent casting and broadened the applicability of vat photopolymerization 3DP. The reprocessability also provides an opportunity for recycling *via* solvent or thermal means. Overall, this work demonstrates several unique advantages of lignin-derived monomers in the development of more sustainable 3DP photoresins for high-performance additive manufacturing.

Materials and Methods

Materials: Triethylamine (≥99.5%), 4-pG, syringol, methacryloyl chloride (97%), acryloyl chloride (97%), Irg 819 (97%), LMA (96%), LA (90%), nile red, dichloromethane (≥99.8%), tetrahydrofuran (≥99.9%), and L-fenchone (≥98%) were all purchased from Sigma Aldrich. Higher purity lauryl acrylate (>98%) and (+/-)limonene (>95%) were purchased from TCI. Chloroform (99.9%), toluene (99.9%), isopropyl alcohol (>99.9%), and *p*-xylene (99.9%) were purchased from Fisher Chemicals. Krytox® GPL103 was purchased from Amazon. All materials were used as received.

Synthesis of monomers: 4-pGA, SMA, and SA were synthesized following a procedure reported in literature.[32] In brief, the respective aromatic monomers and triethylamine (1.2 mol eq) were dissolved in dry dichloromethane in a round-bottom flask. The solution was immersed in an ice-water bath and cooled to 0 °C before (meth)acryloyl chloride (1.4 mol eq) was added drop wise. The cooling bath was then removed, and the solution was stirred unmonitored for 12 h. After the reaction, a white precipitant was filtered out and rinsed with dichloromethane. The organic phase was washed with aqueous solutions of sodium bicarbonate (saturated), 1.0 M NaOH, and 1.0 M HCl. The products were further purified by running through a basic alumina plug and concentrated by rotary evaporation.

3D printing setups: All photoresins were printed on a home-built digital light processing (DLP) 3D printer. For the bottom-up printer, images were projected from an Acer X152H projector. The position of the lens was adjusted so that image could be focused on the bottom of vat, which was about 10 cm away from the lens. For the top-down printer, images were projected from a ViewSonic Projector (PA503S). An extra lens was used to focus the image to the top surface of the photoresin, which was about 15 cm away from the lens. Krytox® GPL103 oil was used to support the photoresin (Figure S1, Figure S2). Creation Workshop was used to slice STL files and control each printer setup. All print files are linked in the Supporting Information.

Top-Down 3D printing of SMA resins: Photoresins were floated on a layer of fluorinated oil (~20 mm thick) and brought to 40 °C using a heated water bath. Print settings included a layer thickness of 0.1 mm and layer cure times of 5 - 35 s. Irgacure 819 was used as the photoinitiator, 4-pG was the inhibitor, and lauryl methacrylate (LMA) was a property modifier. After printing, each test specimen was postcured for 1 h using 405-nm light, followed by thermal curing in an oven for 1 h unless otherwise specified. When printing SMA-2, the incorporation of LMA was assessed by ^{1}H NMR spectroscopy analysis of the uncured photoresin before and after printing, which confirmed equal consumption of SMA and LMA during printing (Figure S13).

Bottom-up 3D printing of 4-pGA resins: Printing involved a bottom-up printer design (images projected from below the resin vat) with a bottom layer of fluorinated oil about 1-mm thick in the vat, layer thicknesses of 0.1 mm, and layer cure times of 10 – 35 s. After printing, each test specimen was postcured at ~20 °C for 1 h using 405-nm light. Analysis of the residual photoresin's composition by ^{1}H NMR spectroscopy confirmed that the composition did not change after printing indicating consistent incorporation of the monomers throughout the printed part (Figure S13).

Mechanical tests: Tensile and compressive tests were conducted on a MTS Criterion® Electromechanical Testing System. For the tensile tests, an ASTM D638 type V specimen was

printed. The strain rate was set to 10 mm/min for more rigid plastics (parts produced from SMA-based photoresins, 4-pGA-1, 4-pGA-2, 4-pGA-6) and 50 mm/min for elastomers (4-pGA-3, 4-pGA-4, and 4-pGA-5). Tensile strain was measured through video analysis by measuring the distance between series of lines that were drawn on the dogbones in the gauge region prior to testing. Strain was calculated based on the change in distance between the lines on the dogbones. Stress-strain curves were obtained by correlating stress and strain values. For the compressive tests, a pillar with a diameter of 5 mm and a height of 10 mm was printed. The compressive rate was set to 1 mm/min.

Nuclear Magnetic Resonance (NMR) spectroscopy: ^{1}H and ^{13}C NMR spectra were obtained using Bruker Avance III 400 or 500 MHz spectrometers. ^{1}H NMR spectra of combined resins were taken using the Bruker Avance III 400 MHz spectrometer, while ^{1}H and ^{13}C NMR spectra were obtained using the Bruker Avance III 500 MHz spectrometer. Chemical shifts are reported in delta (δ) units, expressed in parts per million (ppm) downfield from tetramethylsilane using residual protio-solvent as an internal standard ($CDCl_3$, δH = 7.26 ppm for ^{1}H NMR, δC = 77.16 ppm for ^{13}C NMR) (Figure S13, Figure S14, Figure S15).

Thermogravimetric Analysis (TGA), DSC, and DMA: TGA was conducted on a TA TGA Q50 under nitrogen from room temperature to 600 °C at a rate of 10 °C/min (Figure S16). DSC tests were conducted on a TA DSC Q200 calorimeter under air. Samples were sealed in a Tzero aluminum pan and lid. A heat-cool-heat profile was conducted at a 10 °C/min heating and cooling rate. The temperature range depended on the decomposition temperature determined using TGA and varied between samples. The second heating cycle was used to measure T_g. DMA tests were done on a PerkinElmer DMA 8000. Sinusoidal forces were applied to rectangular samples. The strain was 0.03, frequency was 1 Hz, and heating rate was 3 °C/min.

Gas Chromatography-Mass Spectrometry (GC-MS): GC-MS was conducted on a Shimadzu QP-2020 NX (Shimadzu Corporation) equipped with a MS detector, a flame ionization detector, an AOC-20i autosampler, and a Rtx-5MS column. Samples were dissolved in methanol prior to analysis. The injector temperature was set to 300 °C with a split ratio of 40:1, and the initial oven temperature was set to 50 °C. The oven temperature was held at 50 °C for 1 min before ramping to 315 °C at a rate of 15 °C/min. The MS interface temperature was set to 250 °C with an ion source temperature of 230 °C. GC-MS chromatograms were analyzed using Shimadzu GCMSsolution software (Figure S17).

SEC: Gel-permeation chromatography was conducted on a Tosoh EcoSEC 8320 (Tosoh Bioscience) equipped with a refractive index detector, a TSKgel HHR-H guard column, and two TSKgel GMHHR-N columns in series. The mobile phase was chloroform. The flow rate was 1.00 mL/min, and the temperature was 40 °C. Samples were dissolved in chloroform at a concentration of 1.0 mg/mL for at least 12 h and filtered through 0.1 μm poly(tetrafluoroethylene) syringe filters prior to analysis. A cubic calibration curve of $\log_{10}$(M) vs. retention time was made using a series of 9 polystyrene standards ranging from 589 g/mol to 2,110,000 g/mol (Figure S20) (PStQuick C and PstQuick D, Tosoh Bioscience). All reported molecular weights are polystyrene equivalent molecular weights.

Solvent Casting: Printed parts were first dissolved in dichloromethane. Once fully dissolved, the mixture was poured into silicon molds and left until fully solidified. The parts were then carefully removed from the mold revealing solvent casted pieces.

Acknowledgment

T.H.E. and R.M.O. are grateful for financial support from the National Science Foundation Growing Convergence Research program (NSF GCR CMMI 1934887) in Materials Life-Cycle Management. A.J.B. acknowledges partial financial support from the Yamamoto Family, the Office of the Vice Chancellor for Research and Graduate Education at the University of Wisconsin – Madison with funding from the Wisconsin Alumni Research Foundation, as well as the Army Research Office (W911NF-20-2-0182-P00005-(76555-EG-MUR)). K.C.H.C. and J.C. would like to thank Jacob Zeuske from the Wisconsin Structures and Materials Testing Laboratory for tensile/compressive testing assistance. The following instrumentation in the Paul Bender Chemical Instrumentation Center was supported by: Bruker AVANCE 400 NMR spectrometer by NSF CHE-1048642 and Bruker AVANCE 500 NMR spectrometer by a generous gift from Paul J. and Margaret M. Bender. This work is also supported by a National Science Foundation Graduate Research Fellowship under Grant No. DGE-1747503 to K.C.H.C. Any opinion, findings, and conclusions or recommendations expressed in this material are those of the authors(s) and do not necessarily reflect the views of the National Science Foundation.

References

(1) Javaid, M.; Haleem, A. Additive Manufacturing Applications in Medical Cases: A Literature Based Review. *Alexandria J. Med.* **2018**, *54* (4), 411–422. https://doi.org/10.1016/j.ajme.2017.09.003.

(2) Datta, P.; Ayan, B.; Ozbolat, I. T. Bioprinting for Vascular and Vascularized Tissue Biofabrication. *Acta Biomater.* **2017**, *51*, 1–20. https://doi.org/10.1016/j.actbio.2017.01.035.

(3) Leal, R.; Barreiros, F. M.; Alves, L.; Romeiro, F.; Vasco, J. C.; Santos, M.; Marto, C. Additive Manufacturing Tooling for the Automotive Industry. *Int. J. Adv. Manuf. Technol.* **2017**, *92* (5–8), 1671–1676. https://doi.org/10.1007/s00170-017-0239-8.

(4) Adams, J. J.; Duoss, E. B.; Malkowski, T. F.; Motala, M. J.; Ahn, B. Y.; Nuzzo, R. G.; Bernhard, J. T.; Lewis, J. A. Conformal Printing of Electrically Small Antennas on Three-Dimensional Surfaces. *Adv. Mater.* **2011**, *23* (11), 1335–1340. https://doi.org/10.1002/adma.201003734.

(5) Kim, Y.; Yuk, H.; Zhao, R.; Chester, S. A.; Zhao, X. Printing Ferromagnetic Domains for Untethered Fast-Transforming Soft Materials. *Nature* **2018**, *558* (7709), 274–279. https://doi.org/10.1038/s41586-018-0185-0.

(6) Sachyani Keneth, E.; Kamyshny, A.; Totaro, M.; Beccai, L.; Magdassi, S. 3D Printing Materials for Soft Robotics. *Adv. Mater.* **2021**, *33* (19), 2003387. https://doi.org/10.1002/adma.202003387.

(7) Wallin, T. J.; Pikul, J.; Shepherd, R. F. 3D Printing of Soft Robotic Systems. *Nat. Rev. Mater.* **2018**, *3* (6), 84–100. https://doi.org/10.1038/s41578-018-0002-2.

(8) Lei, M.; Hong, W.; Zhao, Z.; Hamel, C.; Chen, M.; Lu, H.; Qi, H. J. 3D Printing of Auxetic Metamaterials with Digitally Reprogrammable Shape. *ACS Appl. Mater. Interfaces* **2019**, *11* (25), 22768–22776. https://doi.org/10.1021/acsami.9b06081.

(9) Tofail, S. A. M.; Koumoulos, E. P.; Bandyopadhyay, A.; Bose, S.; O'Donoghue, L.; Charitidis, C. Additive Manufacturing: Scientific and Technological Challenges, Market Uptake and Opportunities. *Mater. Today* **2018**, *21* (1), 22–37. https://doi.org/10.1016/j.mattod.2017.07.001.

(10) Appuhamillage, G. A.; Chartrain, N.; Meenakshisundaram, V.; Feller, K. D.; Williams, C. B.; Long, T. E. 110th Anniversary: Vat Photopolymerization-Based Additive Manufacturing: Current Trends and Future Directions in Materials Design. *Ind. Eng. Chem. Res.* **2019**, *58* (33), 15109–15118. https://doi.org/10.1021/acs.iecr.9b02679.

(11) Kelly, B. E.; Bhattacharya, I.; Heidari, H.; Shusteff, M.; Spadaccini, C. M.; Taylor, H. K. Volumetric Additive Manufacturing via Tomographic Reconstruction. *Science* **2019**, *363* (6431), 1075–1079. https://doi.org/10.1126/science.aau7114.

(12) Shusteff, M.; Browar, A. E. M.; Kelly, B. E.; Henriksson, J.; Weisgraber, T. H.; Panas, R. M.; Fang, N. X.; Spadaccini, C. M. One-Step Volumetric Additive Manufacturing of Complex Polymer Structures. *Sci. Adv.* **2017**, *3* (12), eaao5496. https://doi.org/10.1126/sciadv.aao5496.

(13) Zhang, J.; Hu, Q.; Wang, S.; Tao, J.; Gou, M. Digital Light Processing Based Three-Dimensional Printing for Medical Applications. *Int. J. Bioprinting* **2020**, *6* (1), 12–27. https://doi.org/10.18063/ijb.v6i1.242.

(14) Phillips, R. Photopolymerization. *J. Photochem.* **1984**, *25* (1), 79–82. https://doi.org/10.1016/0047-2670(84)85016-9.

(15) Crivello, J. V.; Reichmanis, E. Photopolymer Materials and Processes for Advanced Technologies.

Chem. Mater. **2014**, *26* (1), 533–548. https://doi.org/10.1021/cm402262g.

(16) Boydston, A. J.; Cui, J.; Lee, C. U.; Lynde, B. E.; Schilling, C. A. 100th Anniversary of Macromolecular Science Viewpoint: Integrating Chemistry and Engineering to Enable Additive Manufacturing with High-Performance Polymers. *ACS Macro Lett.* **2020**, *9* (8), 1119–1129. https://doi.org/10.1021/acsmacrolett.0c00390.

(17) Mathers, R. T. How Well Can Renewable Resources Mimic Commodity Monomers and Polymers? *J. Polym. Sci. Part A Polym. Chem.* **2012**, *50* (1), 1–15. https://doi.org/10.1002/pola.24939.

(18) Upton, B. M.; Kasko, A. M. Strategies for the Conversion of Lignin to High-Value Polymeric Materials: Review and Perspective. *Chem. Rev.* **2016**, *116* (4), 2275–2306. https://doi.org/10.1021/acs.chemrev.5b00345.

(19) Wang, H.; Pu, Y.; Ragauskas, A.; Yang, B. From Lignin to Valuable Products–Strategies, Challenges, and Prospects. *Bioresour. Technol.* **2019**, *271*, 449–461. https://doi.org/10.1016/j.biortech.2018.09.072.

(20) Ragauskas, A. J.; Beckham, G. T.; Biddy, M. J.; Chandra, R.; Chen, F.; Davis, M. F.; Davison, B. H.; Dixon, R. A.; Gilna, P.; Keller, M.; Langan, P.; Naskar, A. K.; Saddler, J. N.; Tschaplinski, T. J.; Tuskan, G. A.; Wyman, C. E. Lignin Valorization: Improving Lignin Processing in the Biorefinery. *Science* **2014**, *344* (6185), 1246843. https://doi.org/10.1126/science.1246843.

(21) O'Dea, R. M.; Willie, J. A.; Epps, III, T. H. 100th Anniversary of Macromolecular Science Viewpoint: Polymers from Lignocellulosic Biomass. Current Challenges and Future Opportunities. *ACS Macro Lett.* **2020**, *9* (4), 476–493. https://doi.org/10.1021/acsmacrolett.0c00024.

(22) Mahajan, J. S.; O'Dea, R. M.; Norris, J. B.; Korley, L. T. J.; Epps, III, T. H. Aromatics from Lignocellulosic Biomass: A Platform for High-Performance Thermosets. *ACS Sustain. Chem. Eng.* **2020**, *8* (40), 15072–15096. https://doi.org/10.1021/acssuschemeng.0c04817.

(23) Boerjan, W.; Ralph, J.; Baucher, M. Lignin Biosynthesis. *Annu. Rev. Plant Biol.* **2003**, *54*, 519–546. https://doi.org/10.1146/annurev.arplant.54.031902.134938.

(24) O'Dea, R. M.; Pranda, P. A.; Luo, Y.; Amitrano, A.; Ebikade, E. O.; Gottlieb, E. R.; Ajao, O.; Benali, M.; Vlachos, D. G.; Ierapetritou, M.; Epps, III, T. H. Ambient-Pressure Lignin Valorization to High-Performance Polymers by Intensified Reductive Catalytic Deconstruction. *Sci. Adv.* **2022**, *8* (3), eabj7523. https://doi.org/10.1126/sciadv.abj7523.

(25) Bassett, A. W.; Sweet, K. R.; O'Dea, R. M.; Honnig, A. E.; Breyta, C. M.; Reilly, J. H.; La Scala, J. J.; Epps III, T. H.; Stanzione, J. F. Dual-Functional, Aromatic, Epoxy-Methacrylate Monomers from Bio-Based Feedstocks and Their Respective Epoxy-Functional Thermoplastics. *J. Polym. Sci.* **2020**, *58* (5), 673–682. https://doi.org/10.1002/pol.20190110.

(26) Li, H.; Sun, J. T.; Wang, C.; Liu, S.; Yuan, D.; Zhou, X.; Tan, J.; Stubbs, L.; He, C. High Modulus, Strength, and Toughness Polyurethane Elastomer Based on Unmodified Lignin. *ACS Sustain. Chem. Eng.* **2017**, *5* (9), 7942–7949. https://doi.org/10.1021/acssuschemeng.7b01481.

(27) Liu, W.; Fang, C.; Wang, S.; Huang, J.; Qiu, X. High-Performance Lignin-Containing Polyurethane Elastomers with Dynamic Covalent Polymer Networks. *Macromolecules* **2019**, *52* (17), 6474–6484. https://doi.org/10.1021/acs.macromol.9b01413.

(28) Hernandez, E. D.; Bassett, A. W.; Sadler, J. M.; La Scala, J. J.; Stanzione, J. F. Synthesis and Characterization of Bio-Based Epoxy Resins Derived from Vanillyl Alcohol. *ACS Sustain. Chem.*

Eng. **2016**, *4* (8), 4328–4339. https://doi.org/10.1021/acssuschemeng.6b00835.

(29) Nicastro, K. H.; Kloxin, C. J.; Epps, III, T. H. Potential Lignin-Derived Alternatives to Bisphenol A in Diamine-Hardened Epoxy Resins. *ACS Sustain. Chem. Eng.* **2018**, *6* (11), 14812–14819. https://doi.org/10.1021/acssuschemeng.8b03340.

(30) Zhou, J.; Zhang, H.; Deng, J.; Wu, Y. High Glass-Transition Temperature Acrylate Polymers Derived from Biomasses, Syringaldehyde, and Vanillin. *Macromol. Chem. Phys.* **2016**, *217* (21), 2402–2408. https://doi.org/10.1002/macp.201600305.

(31) Holmberg, A. L.; Reno, K. H.; Nguyen, N. A.; Wool, R. P.; Epps, III, T. H. Syringyl Methacrylate, a Hardwood Lignin-Based Monomer for High-Tg Polymeric Materials. *ACS Macro Lett.* **2016**, *5* (5), 574–578. https://doi.org/10.1021/acsmacrolett.6b00270.

(32) Wang, S.; Shuai, L.; Saha, B.; Vlachos, D. G.; Epps, III, T. H. From Tree to Tape: Direct Synthesis of Pressure Sensitive Adhesives from Depolymerized Raw Lignocellulosic Biomass. *ACS Cent. Sci.* **2018**, *4* (6), 701–708. https://doi.org/10.1021/acscentsci.8b00140.

(33) Çayli, G.; Meier, M. A. R. Polymers from Renewable Resources: Bulk ATRP of Fatty Alcohol-derived Methacrylates. *Eur. J. Lipid Sci. Technol.* **2008**, *110* (9), 853–859. https://doi.org/10.1002/ejlt.200800028.

(34) Meier, M. A. R.; Metzger, J. O.; Schubert, U. S. Plant Oil Renewable Resources as Green Alternatives in Polymer Science. *Chem. Soc. Rev.* **2007**, *36* (11), 1788–1802. https://doi.org/10.1039/b703294c.

(35) Coelho, J. F. J.; Carvalho, E. Y.; Marques, D. S.; Popov, A. V.; Goncalves, P. M.; Gil, M. H. Synthesis of Poly(Lauryl Acrylate) by Single-Electron Transfer/Degenerative Chain Transfer Living Radical Polymerization Catalyzed by Na2S2O4 in Water. *Macromol. Chem. Phys.* **2007**, *208* (11), 1218–1227. https://doi.org/10.1002/MACP.200700015.

(36) Hiemenz, P. C.; Lodge, T. Polymer Chemistry (2nd Edition). **2007**, 587.

(37) Deng, S.; Wu, J.; Dickey, M. D.; Zhao, Q.; Xie, T. Rapid Open-Air Digital Light 3D Printing of Thermoplastic Polymer. *Adv. Mater.* **2019**, *31* (39), 1903970. https://doi.org/10.1002/adma.201903970.

(38) Zhu, S.; Hamielec, A. E. Gel Formation in Free Radical Polymerization via Chain Transfer and Terminal Branching. *J. Polym. Sci. Part B Polym. Phys.* **1994**, *32* (5), 929–943. https://doi.org/10.1002/polb.1994.090320516.

(39) Fox, T. G.; Gratch, S. Crosslinking in Monovinyl Monomers (I). By Chain Transfer With the Polymer Chain. *Ann. N. Y. Acad. Sci.* **1953**, *57* (4), 367–383. https://doi.org/10.1111/j.1749-6632.1953.tb36411.x.

(40) Miller-Chou, B. A.; Koenig, J. L. A Review of Polymer Dissolution. *Prog. Polym. Sci.* **2003**, *28* (8), 1223–1270. https://doi.org/10.1016/S0079-6700(03)00045-5.

(41) Emerson, J. A.; Garabedian, N. T.; Burris, D. L.; Furst, E. M.; Epps, III, T. H. Exploiting Feedstock Diversity to Tune the Chemical and Tribological Properties of Lignin-Inspired Polymer Coatings. *ACS Sustain. Chem. Eng.* **2018**, *6* (5), 6856–6866. https://doi.org/10.1021/acssuschemeng.8b00667.

(42) Post, B. K.; Richardson, B.; Lind, R.; Love, L. J.; Lloyd, P.; Kunc, V.; Rhyne, B. J.; Roschli, A.; Hannan, J.; Nolet, S.; Veloso, K.; Kurup, P.; Remo, T.; Jenne, D. Big Area Additive Manufacturing Application in Wind Turbine Molds. *Solid Free. Fabr. 2017 Proc. 28th Annu. Int.*

Solid Free. Fabr. Symp. - An Addit. Manuf. Conf. SFF 2017 **2020**, 2430–2446.

(43) Le Néel, T. A.; Mognol, P.; Hascoët, J. Y. A Review on Additive Manufacturing of Sand Molds by Binder Jetting and Selective Laser Sintering. *Rapid Prototyp. J.* **2018**, *24* (8), 1325–1336. https://doi.org/10.1108/RPJ-10-2016-0161.

(44) Wang, J.; Sama, S. R.; Lynch, P. C.; Manogharan, G. Design and Topology Optimization of 3D-Printed Wax Patterns for Rapid Investment Casting. *Procedia Manuf.* **2019**, *34*, 683–694. https://doi.org/10.1016/j.promfg.2019.06.224.